Nonlinear Dynamics (2005) 40: 169–193

On the Computer Formulations of the Wheel/Rail Contact Problem

AHMED A. SHABANA*, MAHMOUD TOBAA, HIROYUKI SUGIYAMA,
and KHALED E. ZAAZAA
*Department of Mechanical and Industrial Engineering, University of Illinois at Chicago, 842 West Taylor Street, Chicago, IL 60607-7022, U.S.A.; *Author for correspondence (e-mail: shabana@uic.edu; fax: +1-312-413-0447)*

(Received: 6 July 2004; accepted: 8 October 2004)

Abstract. In this investigation, four nonlinear dynamic formulations that can be used in the analysis of the wheel/rail contact are presented, compared and their performance is evaluated. Two of these formulations employ nonlinear algebraic kinematic constraint equations to describe the contact between the wheel and the rail (constraint approach), while in the other two formulations the contact force is modeled using a compliant force element (elastic approach). The goal of the four formulations is to provide accurate nonlinear modeling of the contact between the wheel and the rail, which is crucial to the success of any computational algorithm used in the dynamic analysis of railroad vehicle systems. In the formulations based on the elastic approach, the wheel has six degrees of freedom with respect to the rail, and the normal contact forces are defined as function of the penetration using Hertz's contact theory or using assumed stiffness and damping coefficients. The first elastic method is based on a search for the contact locations using discrete nodal points. As previously presented in the literature, this method can lead to impulsive forces due to the abrupt change in the location of the contact point from one time step to the next. This difficulty is avoided in the second elastic approach in which the contact points are determined by solving a set of algebraic equations. In the formulations based on the constraint approach, on the other hand, the case of a non-conformal contact is assumed, and nonlinear kinematic contact constraint equations are used to impose the contact conditions at the position, velocity and acceleration levels. This approach leads to a model, in which the wheel has five degrees of freedom with respect to the rail. In the constraint approach, the wheel penetration and lift are not permitted, and the normal contact forces are calculated using the technique of Lagrange multipliers and the augmented form of the system dynamic equations. Two equivalent constraint formulations that employ two different solution procedures are discussed in this investigation. The first method leads to a larger system of equations by augmenting all the contact constraint equations to the dynamic equations of motion, while in the second method an embedding procedure is used to obtain a reduced system of equations from which the surface parameter accelerations are systematically eliminated. Numerical results are presented in order to examine the performance of various methods discussed in this study.

Key words: contact constraint and elastic formulations, multibody dynamics, railroad vehicle dynamics, wheel/rail contact

1. Introduction

In railroad vehicle dynamics, accurate prediction of the location of the contact point is crucial in any algorithm developed to solve the dynamics of wheel/rail contact problems [1–7]. There are, in general, two different approaches used to solve the wheel/rail contact problems. The first approach is the contact constraint approach in which the contact between the wheel and rail surfaces is described using nonlinear algebraic kinematic constraint equations. These equations can be solved with the equations of motion using the techniques of Lagrange multipliers and the augmented form of the dynamic equations. The normal contact forces are determined in this formulation as constraint forces associated with the contact constraints. Since the wheel and rail are assumed in this constraint formulation to remain in contact, the wheel has five degrees of freedom with respect to the rail and the wheel lift is not, in general, allowed [8]. The second approach used is the elastic contact formulation. In this formulation, the normal contact forces are modeled using compliant forces based on the Hertzian contact theory or using an assumed

compliant force model. Small local deformations in the contact area are used to define the normal contact force.

The constraint and elastic contact formulations lead to different forms of the equations of motion that require the use of different numerical solution procedures. In the case of the constraint formulation, the equations of motion are expressed in terms of a set of surface parameters that describe the geometry of the surfaces of the wheel and rail in contact as will be discussed in Section 2. For this reason, the system equations are solved for the wheel and rail coordinates and the surface parameters as well as the vector of Lagrange multipliers that is used to determine the normal contact forces. On the other hand, in the elastic contact formulation, the equations of motion for the wheel/rail contact problem are expressed in terms of wheel and rail coordinates only, and the contact forces are treated as generalized external forces defined at the contact point. Since no kinematic contact constraints are imposed in this formulation, accurate prediction of the location of the contact point is crucial and some geometrical problems need to be addressed. A general search procedure to solve the general three dimensional wheel/rail contact problems has been recently proposed [9]. The idea of the search method is to use a set of discrete nodal points on the wheel and rail surfaces to check whether or not penetration occurs between the two bodies. This procedure that does not require a certain degree of smoothness of the contact surfaces can be applied to any profile of body surfaces. Despite the generality of the method, a large number of nodal points is required in order to accurately predict the location of the contact points. Another problem encountered in using this method is due to the fact that the change in the location of the contact points is not continuous as the result of using discrete nodal points. Such an abrupt change can, in some examples, lead to discontinuities in the velocities at the contact points which in turns lead to discontinuity in the creepages and significant jump discontinuities in the creep forces as the result of the high values of the creepage coefficients.

In this paper, several constraint and elastic contact formulations for multibody railroad vehicle applications are discussed and suggestions to improve accuracy and efficiency of existing formulations are proposed. In particular, a solution procedure for the constraint formulation that systematically eliminates all the surface parameter accelerations from the equations of motion is developed. In the case of the elastic contact formulations, a procedure that can be used to determine the location of the contact point is proposed. In this procedure, a set of algebraic equations instead of discrete nodal points is used in order to avoid the use of discrete nodal search that leads to impulsive creep forces. The use of algebraic equations leads to a smoother and more efficient solution in the case of smooth wheel and rail profiles.

The work presented in this study can be considered as an extension of the analysis and comparative study presented in [9]. The work presented in this study, however, differs from previously published work since it discusses two contact formulations that were not discussed in [9]. One of these formulations is the embedded contact constraint formulation (ECCF) and the other is an elastic contact formulation referred to as ECF-A. Numerical experimentation showed that these two formulations can be used to develop accurate and robust computer algorithms and provide alternatives for the two constraint and elastic formulations discussed in [9]. This paper is organized as follows: The parameterization of the wheel and rail surfaces is briefly discussed in Section 2. Two different contact constraint formulations are introduced in Section 3, while the elastic formulations are presented in Section 4. Numerical results obtained using a full vehicle model are presented in Section 5 in order to demonstrate the use of the formulations discussed in this paper. The results of the two-point contact and curving analysis obtained using the constraint and elastic approaches are compared in Section 6. Summary and conclusions drawn from this study are presented in Section 7.

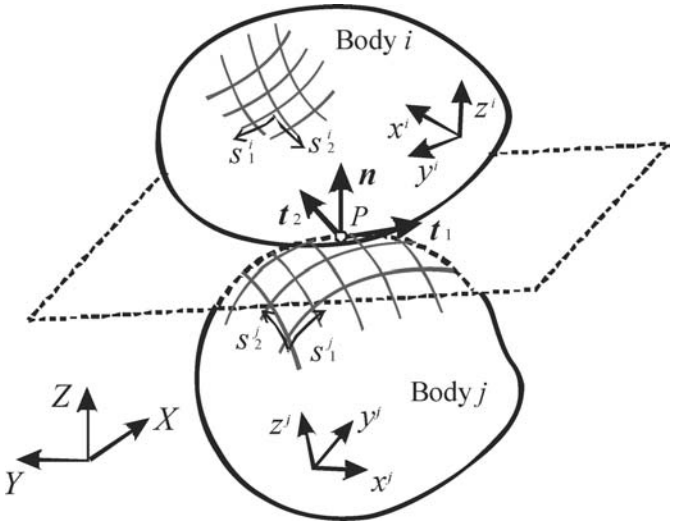

Figure 1. Schematic representation of two bodies in contact.

2. Parameterization of Wheel and Rail Surfaces

In order to determine the location of the point of contact between two bodies, a complete parameterization of the surfaces must be used [8, 10]. In general, a set of four surface parameters is used to describe the geometry of the two surfaces in contact as shown in Figure 1. The surface parameters can be written in a vector form as

$$\mathbf{s} = \left[s_1^i \; s_2^i \; s_1^j \; s_2^j\right]^T \tag{1}$$

where superscripts i and j denotes body i and body j, respectively. Using these parameters, the location of the contact point P can be defined in the body coordinate systems as

$$\bar{\mathbf{u}}_p^i\left(s_1^i, s_2^i\right) = \begin{bmatrix} \bar{x}^i\left(s_1^i, s_2^i\right) \\ \bar{y}^i\left(s_1^i, s_2^i\right) \\ \bar{z}^i\left(s_1^i, s_2^i\right) \end{bmatrix}, \quad \bar{\mathbf{u}}_p^j\left(s_1^j, s_2^j\right) = \begin{bmatrix} \bar{x}^j\left(s_1^j, s_2^j\right) \\ \bar{y}^j\left(s_1^j, s_2^j\right) \\ \bar{z}^j\left(s_1^j, s_2^j\right) \end{bmatrix} \tag{2}$$

The tangents to the surface at the contact point are defined in the body coordinate system as

$$\bar{\mathbf{t}}_1^i = \frac{\partial \bar{\mathbf{u}}_p^i}{\partial s_1^i}, \quad \bar{\mathbf{t}}_2^i = \frac{\partial \bar{\mathbf{u}}_p^i}{\partial s_2^i} \tag{3}$$

and the normal vector as

$$\bar{\mathbf{n}}^i = \bar{\mathbf{t}}_1^i \times \bar{\mathbf{t}}_2^i \tag{4}$$

This parameterization can be used to describe the wheel and rail surfaces.

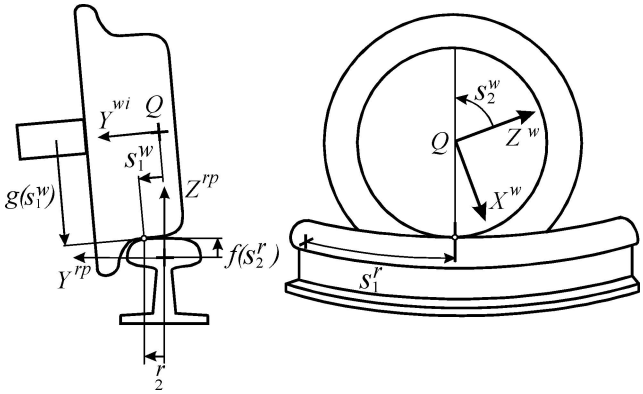

Figure 2. Surface parameters.

2.1. TRACK GEOMETRY

The surface geometry of the rail r can be described in the most general form using the two surface parameters s_1^r and s_2^r, where s_1^r represents the rail arc length and s_2^r is the surface parameter that defines the rail profile, as shown in Figure 2. The surface parameters s_1^r and s_2^r are defined in a profile coordinate system $X^{rp}Y^{rp}Z^{rp}$ shown in Figure 3. The location of the origin and the orientation of the profile coordinate system, defined respectively by the vector $\mathbf{R}^{rp}$ and the transformation matrix $\mathbf{A}^{rp}$, can be uniquely determined using the surface parameter s_1^r [8–10]. Using this description, the global position vector of an arbitrary point on the surface of the rail r can be written as follows:

$$\mathbf{r}^r = \mathbf{R}^r + \mathbf{A}^r(\mathbf{R}^{rp} + \mathbf{A}^{rp}\bar{\mathbf{u}}^{rp}) \tag{5}$$

where $\mathbf{R}^r$ is the global position vector of the origin of the rail coordinate system $X^rY^rZ^r$, $\mathbf{A}^r$ is the transformation matrix that defines the orientation of the rail coordinate system, and $\bar{\mathbf{u}}^{rp}$ is the local position vector that defines the location of the arbitrary point on the rail surface with respect to the profile coordinate system. The location and orientation of the rail profile coordinate system depends only on the distance traveled along the track s_1^r, while the local position of an arbitrary point on the rail

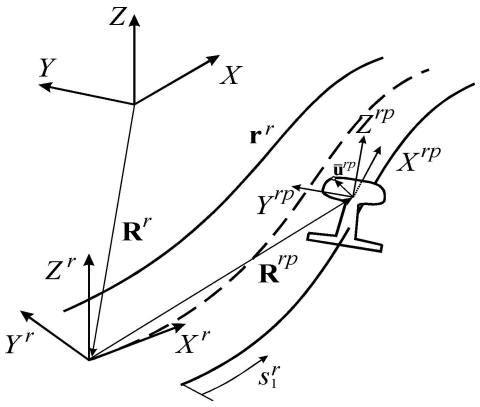

Figure 3. Track geometry.

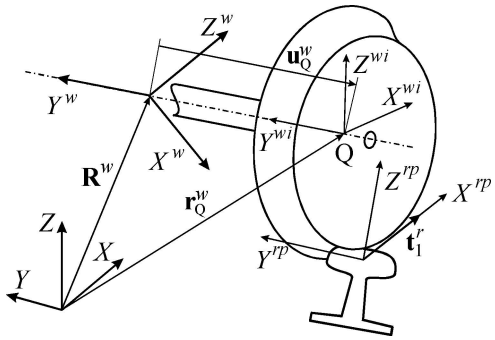

Figure 4. Wheel geometry.

surface at any section depends on the value of s_2^r, that

$$\mathbf{R}^{rp} = \mathbf{R}^{rp}\left(s_1^r\right), \quad \mathbf{A}^{rp} = \mathbf{A}^{rp}\left(s_1^r\right), \quad \bar{\mathbf{u}}^{rp} = \begin{bmatrix} 0 & s_2^r & f\left(s_2^r\right) \end{bmatrix}^T \tag{6}$$

where f is the function that defines the rail profile.

2.2. Wheel Geometry

The geometry of the wheel surface can be described using the two surface parameters s_1^w and s_2^w. These surface parameters are defined in a wheel set coordinate system $X^w Y^w Z^w$. The surface parameter s_1^w defines the wheel profile and s_2^w represents the rotation of the contact point, as shown in Figure 2. The location of the origin and the orientation of the wheel set coordinate system are defined, respectively, by the vector $\mathbf{R}^w$ and the transformation matrix $\mathbf{A}^w$. Using this description, the global position vector of an arbitrary point on the surface of the wheel w can be written as follows:

$$\mathbf{r}^w = \mathbf{R}^w + \mathbf{A}^w \bar{\mathbf{u}}^w \tag{7}$$

where $\bar{\mathbf{u}}^w$ is the local position vector that defines the location of the arbitrary point on the wheel surface with respect to the wheel set coordinate system. In the case of the right wheel, this vector is defined as

$$\bar{\mathbf{u}}^w = \begin{bmatrix} g\left(s_1^w\right)\sin s_2^w & -L + s_1^w & g\left(s_1^w\right)\cos s_2^w \end{bmatrix}^T \tag{8}$$

where g is the function that defines the wheel profile, and L is the distance between the origin of the wheel set coordinate system and point Q of the wheel, as shown in Figures 2 and 4.

3. Contact Constraint Formulations

In this investigation, two contact constraint formulations and two elastic contact formulations are discussed. As described in Section 2, the geometry of the surfaces of the wheel and rail are parameterized using the surface parameters that can be used to define the location of the contact point. In the constraint formulations, the contact between two surfaces can be described using a set of nonlinear algebraic equations that must be imposed at the position, velocity, and acceleration levels. One may choose not to

eliminate the surface parameters, leading to an augmented form of the equations of motion expressed in terms of Lagrange multipliers associated with the kinematic contact constraint equations. This *augmented contact constraint formulation* will be referred to in this study as ACCF. Alternatively, one may choose to systematically eliminate the surface parameters using the contact constraints, leading to an embedding formulation of the equations of motion that does not explicitly include the surface parameter accelerations. This *embedded contact constraint formulation* will be referred to in this study as ECCF. Both ACCF and ECCF, which are conceptually equivalent but employ different solution algorithms and numerical procedures, will be discussed in this section.

3.1. Contact Constraints

When two rigid bodies come in contact as schematically represented by Figure 1, two non-conformal kinematic contact conditions need to be satisfied [8]. First, two points (contact points) on the two surfaces coincides; and second, the two surfaces must have the same tangent planes at the contact point. These two conditions define the following five constraint equations that are required to describe the non-conformal contact between the wheel and rail:

$$\mathbf{C}^k(\mathbf{q}^w, \mathbf{q}^r, \mathbf{s}^{wk}, \mathbf{s}^{rk}) = \begin{bmatrix} \mathbf{r}_P^w - \mathbf{r}_P^r \\ \mathbf{t}_1^w \cdot \mathbf{n}^r \\ \mathbf{t}_2^w \cdot \mathbf{n}^r \end{bmatrix}^k = \mathbf{0} \tag{9}$$

or equivalently,

$$\mathbf{C}^k(\mathbf{q}^w, \mathbf{q}^r, \mathbf{s}^{wk}, \mathbf{s}^{rk}) = \begin{bmatrix} \mathbf{t}_1^r \cdot \left(\mathbf{r}_P^w - \mathbf{r}_P^r\right) \\ \mathbf{t}_2^r \cdot \left(\mathbf{r}_P^w - \mathbf{r}_P^r\right) \\ \mathbf{n}^r \cdot \left(\mathbf{r}_P^w - \mathbf{r}_P^r\right) \\ \mathbf{t}_1^w \cdot \mathbf{n}^r \\ \mathbf{t}_2^w \cdot \mathbf{n}^r \end{bmatrix}^k = \mathbf{0} \tag{10}$$

where superscript k denotes the contact number, superscript r and w denote rail and wheel, respectively, $\mathbf{q}^w$ and $\mathbf{q}^r$ are, respectively, the generalized coordinates of wheel and rail, and $\mathbf{t}_1$, $\mathbf{t}_2$ and $\mathbf{n}$ are the two tangents and normal to the surface at the contact point. In Equation (10), the three relative displacement constraints (point constraints) are defined in a rail coordinate system at the contact point. The first three point constraints of Equation (9), on the other hand, are defined in the global coordinate system.

Using the principle of virtual work in dynamics, the following variational equation of motion can be obtained [8]:

$$\delta\mathbf{q}^T \left(\mathbf{M}\ddot{\mathbf{q}} + \mathbf{C}_\mathbf{q}^T\boldsymbol{\lambda} - \mathbf{Q}\right) + \delta\mathbf{s}^T\mathbf{C}_\mathbf{s}^T\boldsymbol{\lambda} = 0 \tag{11}$$

where the vectors $\mathbf{q}$ and $\mathbf{s}$ are, respectively, the system generalized coordinates and the system surface parameters, $\mathbf{M}$ is a system mass matrix, $\mathbf{Q}$ is a system generalized force vector, $\mathbf{C}_\mathbf{q}$ and $\mathbf{C}_\mathbf{s}$ are, respectively, the constraint Jacobian matrices resulting from the differentiation with respect to the vectors $\mathbf{q}$ and $\mathbf{s}$, and $\boldsymbol{\lambda}$ is the vector of Lagrange multipliers associated with joint and contact constraints. It is important to note that there are no inertia and generalized forces associated with the surface parameters

used to describe the surface geometry; and for this reason these parameters are treated as non-generalized coordinates [8].

Differentiating all the constraint equations twice with respect to time, the constraint equations at the acceleration level can be written as

$$\mathbf{C_q}\ddot{\mathbf{q}} + \mathbf{C_s}\ddot{\mathbf{s}} = \mathbf{Q}_c \tag{12}$$

where $\mathbf{Q}_c$ is a quadratic velocity vector resulting from the differentiation of the constraint equations twice with respect to time.

3.2. Augmented Contact Constraint Formulation (ACCF)

In the contact constraint formulation, the system differential equations of motion and the wheel/rail contact constraint equations are solved simultaneously for the system generalized coordinates and the system surface parameters in order to correctly account for the kinematic and dynamic coupling between the wheel/rail generalized coordinates and the non generalized surface parameters. To this end, Equations (11) and (12) can be used to obtain the following augmented matrix form using the techniques of Lagrange multipliers [8]:

$$\begin{bmatrix} \mathbf{M} & \mathbf{0} & \mathbf{C}_\mathbf{q}^T \\ \mathbf{0} & \mathbf{0} & \mathbf{C}_\mathbf{s}^T \\ \mathbf{C_q} & \mathbf{C_s} & \mathbf{0} \end{bmatrix} \begin{bmatrix} \ddot{\mathbf{q}} \\ \ddot{\mathbf{s}} \\ \boldsymbol{\lambda} \end{bmatrix} = \begin{bmatrix} \mathbf{Q} \\ \mathbf{0} \\ \mathbf{Q}_c \end{bmatrix} \tag{13}$$

As can be seen from Equation (13), the solution vector contains not only the generalized accelerations and the Lagrange multipliers, but also the second time derivatives of the non-generalized surface parameters. These augmented equations of motion are solved for the generalized and non-generalized accelerations and the Lagrange multipliers [8]. Equation (13) ensures that the generalized and non-generalized accelerations automatically satisfy the contact constraints at the acceleration level. Having obtained the acceleration vectors, the independent accelerations that may include the generalized and/or non-generalized variables are identified using the constraint Jacobian matrix. These independent accelerations are integrated forward in time in order to determine the independent coordinates and velocities, and the dependent generalized and non-generalized coordinates can be determined by solving the constraint equations at the position level using a Newton–Raphson iterative solution procedure. The constraint equations at the velocity level are solved to determine the dependent generalized and non-generalized velocities. It is important to point out again that in this method (ACCF), generalized and/or non-generalized coordinates (surface parameters) can be selected as the independent variables, and the state equations associated with these independent variables are integrated forward in time. This is one of the important differences between this method (ACCF) and the method discussed below.

3.3. Embedded Contact Constraint Formulation (ECCF)

In the embedded contact constraint formulations (ECCF), the surface parameters (the non-generalized coordinates) are systematically eliminated from the equations of motion. This leads to a smaller system of equations from which the contact constraint forces (except for the normal contact force) are eliminated.

Before providing the details of this elimination, it is important to comment on Equation (13) that includes for each contact the following four algebraic equations in the five unknown Lagrange multipliers [8]:

$$\mathbf{C}_{\mathbf{s}}^{k^T} \boldsymbol{\lambda}^k = \mathbf{0}; \tag{14}$$

where

$$\mathbf{s}^k = \begin{bmatrix} s_1^{wk} & s_2^{wk} & s_1^{rk} & s_2^{rk} \end{bmatrix}^T; \quad \boldsymbol{\lambda}^k = \begin{bmatrix} \lambda_1^k & \lambda_2^k & \lambda_3^k & \lambda_4^k & \lambda_5^k \end{bmatrix}^T$$

Equation (14) shows that the five Lagrange multipliers associated with each contact are not totally independent, but only one Lagrange multiplier is independent. This result is consistent with the fact that the contact constraints eliminate one degree of freedom and the normal contact force can be expressed in terms of one Lagrange multiplier only.

In order to systematically eliminate the four surface parameters of each contact, four contact constraints are selected from the five contact constraints such that their Jacobian matrix associated with the four surface parameters leads to a non-singular square matrix. Since the degree of freedom eliminated by the contact constraints can be in general the relative motion along the normal to the surface at the contact point, we choose the four constraint equations from Equation (10) by excluding the third equation that defines the relative motion along the normal. This third equation will be augmented to the system differential equations in order to determine the normal force. To this end, the vector of constraint equations associated with contact k is written in the following partitioned form:

$$\mathbf{C}^k(\mathbf{q}^w, \mathbf{q}^r, \mathbf{s}^{wk}, \mathbf{s}^{rk}) = \begin{bmatrix} \mathbf{C}^{dk^T} & C^{nk^T} \end{bmatrix}^T \tag{15}$$

where

$$\mathbf{C}^{dk}(\mathbf{q}^w, \mathbf{q}^r, \mathbf{s}^{wk}, \mathbf{s}^{rk}) = \begin{bmatrix} \mathbf{t}_1^r \cdot \left(\mathbf{r}_P^w - \mathbf{r}_P^r\right) \\ \mathbf{t}_2^r \cdot \left(\mathbf{r}_P^w - \mathbf{r}_P^r\right) \\ \mathbf{t}_1^w \cdot \mathbf{n}^r \\ \mathbf{t}_2^w \cdot \mathbf{n}^r \end{bmatrix}^k = \mathbf{0} \tag{16}$$

$$C^{nk}(\mathbf{q}^w, \mathbf{q}^r, \mathbf{s}^{wk}, \mathbf{s}^{rk}) = \mathbf{n}^{rk} \cdot \left(\mathbf{r}_P^{wk} - \mathbf{r}_P^{rk}\right) = 0 \tag{17}$$

It should be noted that since the Jacobian matrix associated with the constraints of Equation (16) is non-singular, as can be verified, all the four surface parameters can be expressed in terms of the wheel/rail generalized coordinates. However, since the wheel/rail generalized coordinates must satisfy the fifth contact constraint (Equation (17)) as well as other kinematic constraints imposed on the motion of the multibody vehicle system, the position analysis involves two coupled stages, each of which requires the use of the iterative Newton–Raphson procedure. For a given set of wheel/rail generalized coordinates, Equation (16) is solved iteratively using a Newton–Raphson algorithm in order to determine the surface parameters that enter into the formulations of Equation (17). For these calculated surface parameters, Equation (17) and other nonlinear kinematic constraints imposed on the motion of the multibody system are iteratively solved using a Newton–Raphson algorithm in order to determine the system generalized coordinates. This iterative process continues until convergence is achieved for both stages.

Since the four contact constraints of Equation (16) do not prevent the penetration along the normal to the surfaces at the contact point, the fifth constraint of Equation (17) ensures that such a penetration does not occur. Substituting Equation (15) into Equation (11), the variational equations of motion can now be rewritten as

$$\delta\mathbf{q}^T\left(\mathbf{M}\ddot{\mathbf{q}} + \mathbf{C}_{\mathbf{q}}^{d^T}\boldsymbol{\lambda}^d + \mathbf{C}_{\mathbf{q}}^{n^T}\boldsymbol{\lambda}^n - \mathbf{Q}\right) + \delta\mathbf{s}^T\left(\mathbf{C}_{\mathbf{s}}^{d^T}\boldsymbol{\lambda}^d + \mathbf{C}_{\mathbf{s}}^{n^T}\boldsymbol{\lambda}^n\right) = 0 \tag{18}$$

where $\mathbf{C}_s^d$ and $\mathbf{C}_s^n$ are the Jacobian matrices associated with the contact constraints of the types presented in Equations (16) and (17) respectively; and $\boldsymbol{\lambda}^d$ and $\boldsymbol{\lambda}^n$ are the Lagrange multipliers associated with these constraint equations. Note that the virtual change in the system surface parameters can be expressed in terms of the virtual change in the wheel/rail coordinates as follows:

$$\delta\mathbf{s} = \mathbf{B}\delta\mathbf{q} \tag{19}$$

where $\mathbf{B} = -(\mathbf{C}_{\mathbf{s}}^d)^{-1}\mathbf{C}_{\mathbf{q}}^d$ is the velocity transformation matrix associated with the contact constraints. Substituting Equation (19) into Equation (18), the variational equations of motion can then be written in terms of the virtual changes in the generalized coordinates only as

$$\delta\mathbf{q}^T\left(\mathbf{M}\ddot{\mathbf{q}} + \left(\mathbf{C}_{\mathbf{q}}^n + \mathbf{C}_{\mathbf{s}}^n\mathbf{B}\right)^T\boldsymbol{\lambda}^n - \mathbf{Q}\right) = 0 \tag{20}$$

It is important to note in Equation (20) that the generalized contact forces associated with the contact constraints of Equation (16), are systematically eliminated from the equations of motion using the following identity:

$$\mathbf{C}_{\mathbf{q}}^{dT}\boldsymbol{\lambda}^d + \mathbf{B}^T\mathbf{C}_{\mathbf{s}}^{dT}\boldsymbol{\lambda}^d = \mathbf{C}_{\mathbf{q}}^{dT}\boldsymbol{\lambda}^d + \left(-\left(\mathbf{C}_{\mathbf{s}}^d\right)^{-1}\mathbf{C}_{\mathbf{q}}^d\right)^T\mathbf{C}_{\mathbf{s}}^{dT}\boldsymbol{\lambda}^d = \mathbf{0} \tag{21}$$

Furthermore, the acceleration kinematic equation

$$\ddot{\mathbf{s}} = \mathbf{B}\ddot{\mathbf{q}} + \dot{\mathbf{B}}\dot{\mathbf{q}} \tag{22}$$

which is the result of Equation (19), can be used to eliminate $\ddot{\mathbf{s}}$ from the second derivative of the constraint of Equation (17) with respect to time. Using this procedure, one can show that the system equations of motion, after eliminating the non-generalized surface parameters, can be written as

$$\begin{bmatrix} \mathbf{M} & \mathbf{H}^T \\ \mathbf{H} & \mathbf{0} \end{bmatrix}\begin{bmatrix} \ddot{\mathbf{q}} \\ \boldsymbol{\lambda} \end{bmatrix} = \begin{bmatrix} \mathbf{Q} \\ \mathbf{Q}_{cn} \end{bmatrix} \tag{23}$$

where $\mathbf{H}$, an implicit function of $\mathbf{s}$, is the Jacobian matrix of the constraint of Equation (17) and other constraints imposed in the motion of the multibody system, $\boldsymbol{\lambda}$ is the vector of the system Lagrange multipliers that include only Lagrange multipliers associated with the constraints of Equation (17) and other non-contact constraints imposed on the motion of the system, and $\mathbf{Q}_{cn}$ is a quadratic velocity vector that results from the differentiation of the constraint equations twice with respect to time. This vector is a function of the surface parameters $\mathbf{s}$ and their first time derivatives.

It is clear that in the ECCF, the surface parameters are treated as dependent variables and are systematically eliminated from the equations of motion. For this reason, only wheel/rail accelerations are integrated forward in time. It should also be noted that only one Lagrange multiplier associated

with the contact constraint of Equation (17) is used in Equation (23) This Lagrange multiplier defines the normal contact force used to define the longitudinal, lateral and spin creep forces. Furthermore, since the surface parameters and the dependent Lagrange multipliers are systematically eliminated without making any assumptions, the ECCF as defined by Equation (23) and the augmented contact constraint formulation (ACCF) as defined by Equation (13) are in principle equivalent despite the fact that these two formulations require the use of different solution procedures and numerical algorithms.

3.4. Comparison Between the Two Methods

While as previously pointed out the two methods ACCF and ECCF are in principle the same, the use of the surface parameters as degrees of freedom in the ACCF method requires the use of different solution algorithm as compared to the ECCF method. In order to compare between the two methods, the suspended wheel set shown in Figures 5 and 6 is used. The data for this wheel set are shown in Table 1. The wheels are profiled with approximate conicity of 1/40. Cubic splines are used to interpolate the profile data. The wheel set is assumed to have a constant forward velocity of 40 m/s. The left rail is assumed to be perfectly straight, while the right rail has a deviation that defines a sinusoidal gage reduction of 10 mm between two points located at a distance 20 and 30 m on the rail. Figures 7 and 8 show the lateral and yaw displacement of the wheel set as a function of the distance traveled. The results presented in these two figures show that the motion of the wheel set is stable and the lateral and yaw displacements approach zero as the distance traveled increases. Figure 9 shows the normal contact force acting on the right wheel, while Figure 10 shows the normal force acting on the left wheel. While the results presented in these figures show a very good agreement between the solutions obtained using the ACCF and ECCF methods, it is important to point out that numerical experimentation showed that the ECCF method is more robust and less sensitive to changes in the numerical tolerances, while the ACCF method is more sensitive to numerical tolerances. The elimination of the surface parameters in the ECCF method seems to provide a numerical advantage since these parameters cannot be in this

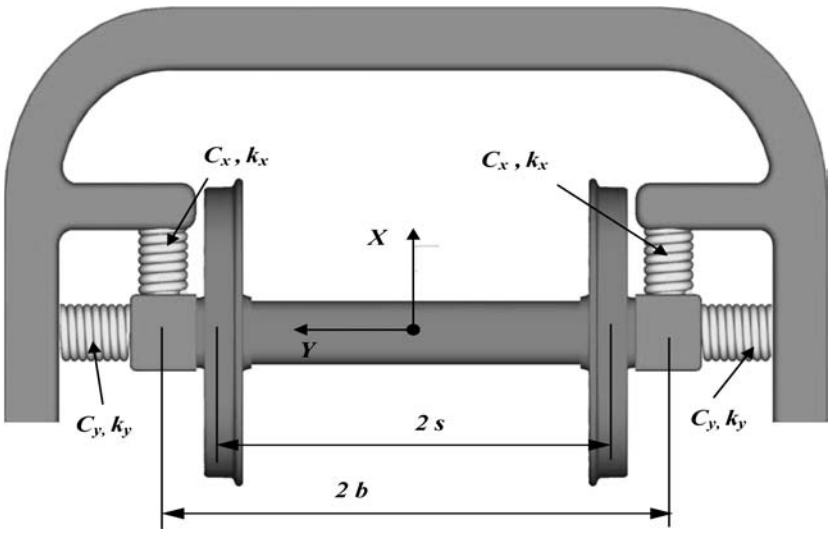

Figure 5. Top view of the suspended wheel set.

Table 1. Data used in the suspended wheel set model.

Variable	Description	Value
m_w	Wheel set mass	1568 kg
I_{xx}	Inertia moment	656 kg · m^2
I_{yy}	Inertia moment	168 kg · m^2
I_{zz}	Inertia moment	656 kg · m^2
W	Applied vertical load	98000 N
k_x	Stiffness for longitudinal springs	1.35×10^5 N/m
k_y	Stiffness for lateral springs	2.5×10^5 N/m
c_x	Damping coefficient for longitudinal spring	1.0×10^5 N/m·s
c_y	Damping coefficient for lateral spring	0 N/m · s
b	Distance between longitudinal springs	0.9 m
$2s$	Gage value	1432 mm

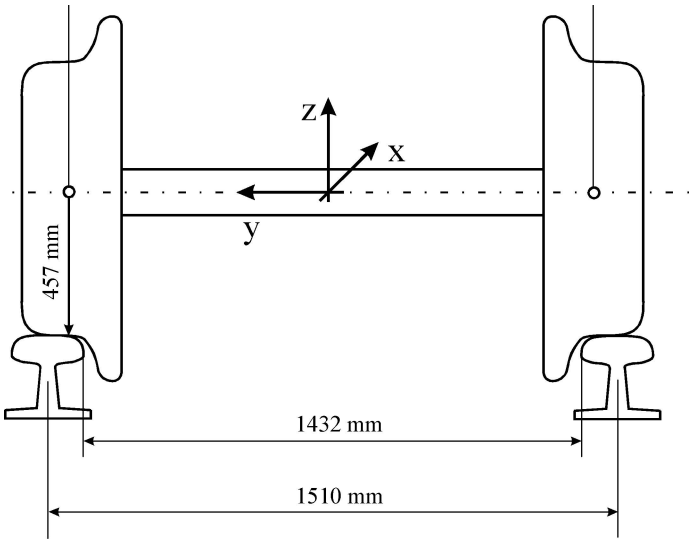

Figure 6. Geometry of wheel set and rails.

case selected by the multibody computer code as independent variables. Furthermore, the size of the coefficient matrices used in solving for the positions, velocities, and accelerations of the wheel set is reduced; thereby minimize the possibility of ill-conditionings and other numerical problems that arise from the use of a large system that combines both generalized and non-generalized variables.

4. Elastic Contact Formulations

The constraint approach does not allow penetration between the two bodies in contact, and imposing the contact conditions eliminates one degree of relative motion between the wheel and the rail. In the elastic approach, on the other hand, no kinematic contact constraints are imposed, the wheel has six degrees of freedom with respect to the rail, and small penetrations at the contact points are allowed. In the elastic contact formulations, a compliant force element that consists of stiffness and damping forces

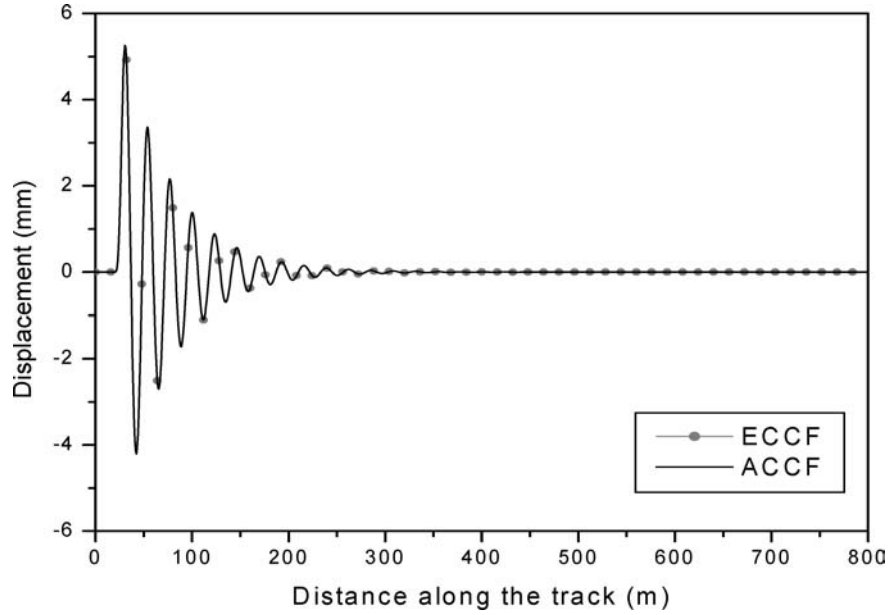

Figure 7. Lateral displacement of the wheel set.

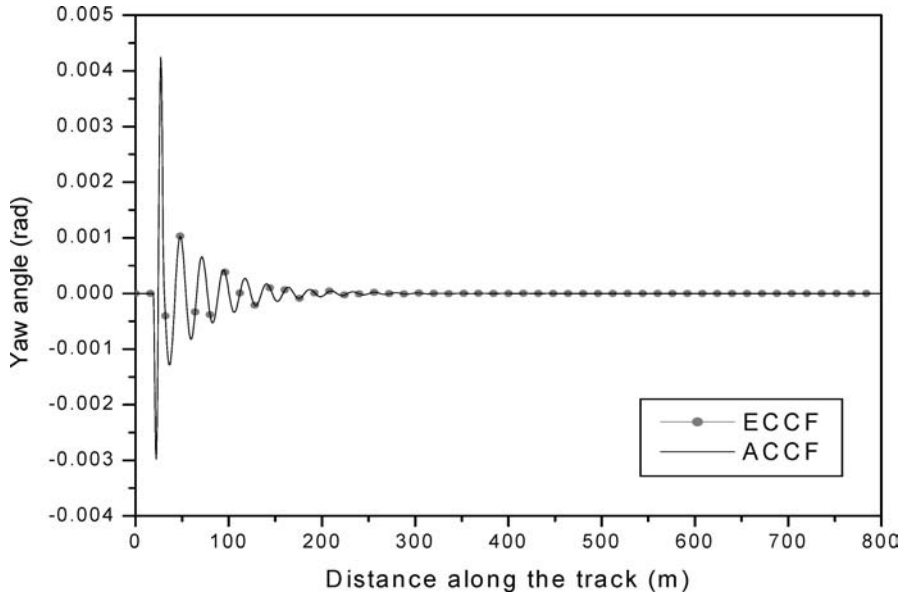

Figure 8. Yaw angle of the wheel set.

is used to determine the normal contact force. The location of the points of contact can be determined using look-up tables, discrete nodal search, or by solving a set of algebraic equations. In this section, two elastic contact formulations are discussed. In the first, called ECF-A, the locations of the contact points are determined by solving a set of algebraic equations. In the second elastic contact method, called ECF-N, the locations of the contact points are determined using the nodal search.

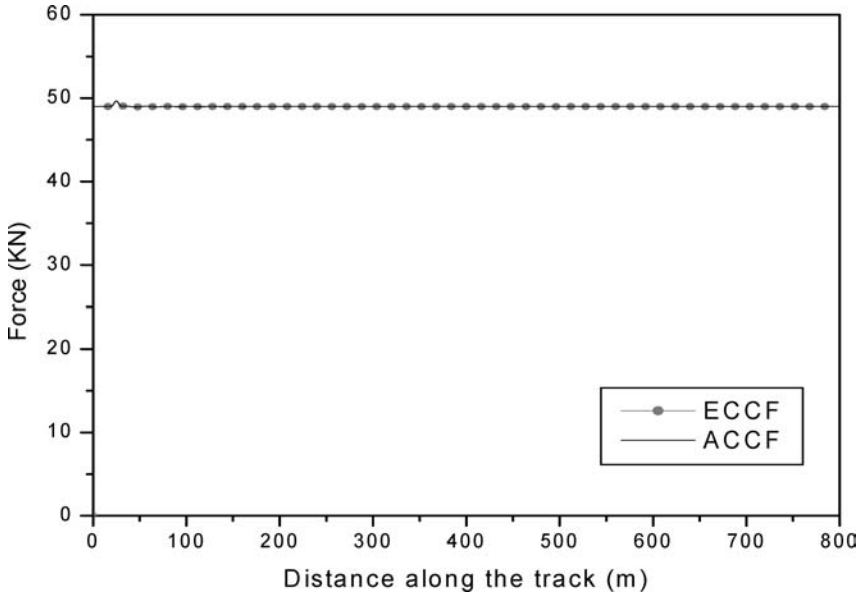

Figure 9. Normal contact forces of the right wheel.

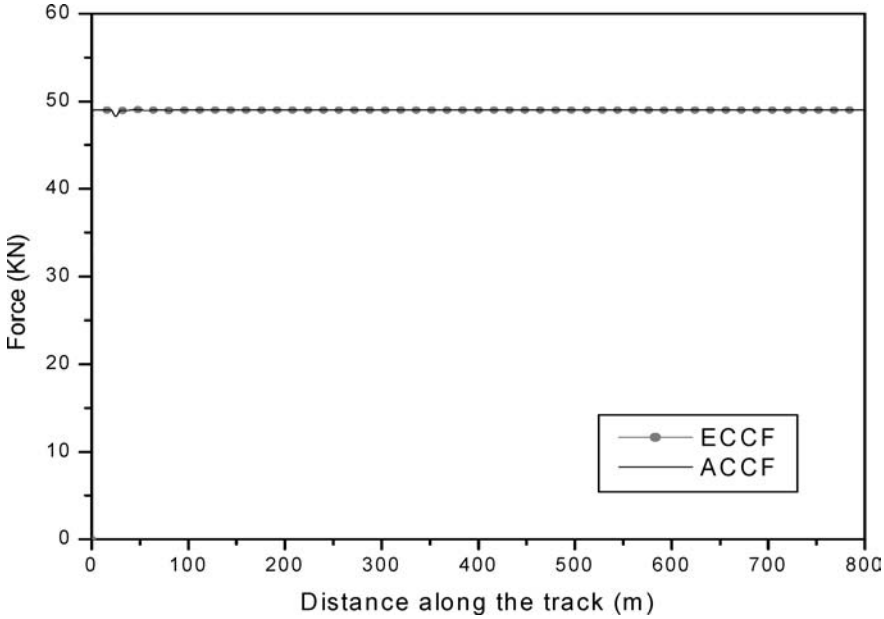

Figure 10. Normal contact forces of the left wheel.

4.1. Use of Algebraic Equations (ECF-A)

In the first elastic method discussed in this section, the locations of the contact points are determined by first solving a set of algebraic equations. For each contact four algebraic equations are solved in order to determine the four surface parameters that describe the geometry of the wheel and the rail surfaces.

After determining the four surface parameters that satisfy the algebraic nonlinear equations, the distance between the surfaces along the normal is evaluated using a fifth equation to determine whether or not there is a contact. The method presented in this section allows for the definition of the wheel and rail surfaces using spline function representations, thereby enabling the use of measured profile data for the wheel and the rail.

It is important to point out that while the algebraic equations used in this method are the same as the contact constraints presented in the preceding section, the method presented in this section (ECF-A) is not considered as a contact constraint formulation since the algebraic equations are not imposed at the velocity and acceleration levels, allow for penetrations, and do not introduce a Lagrange multiplier that is used in the constraint method to determine the normal contact force. In the elastic methods discussed in this section, the normal contact force is determined using a compliant force that has stiffness and damping coefficients.

In order to determine the location of contact point using the elastic contact approach, one may define the following four algebraic equations ([11], J.L. Escalona, personal communication [2002]):

$$\left.\begin{aligned} \mathbf{t}_1^r \cdot \mathbf{r}^{wr} &= 0 \\ \mathbf{t}_2^r \cdot \mathbf{r}^{wr} &= 0 \\ \mathbf{t}_1^w \cdot \mathbf{n}^r &= 0 \\ \mathbf{t}_2^w \cdot \mathbf{n}^r &= 0 \end{aligned}\right\} \tag{24}$$

where $\mathbf{t}_1^k$ and $\mathbf{t}_2^k$ $(k = w, r)$ are, respectively, the tangents to the wheel and rail surfaces at the potential contact point, $\mathbf{r}^{wr} = \mathbf{r}^w - \mathbf{r}^r$ is the vector between two points that can come into contact, and $\mathbf{n}^r$ is the normal to the rail surface. Note that the first two equations in the preceding equation are the same as the first two equations in Equation (10), while the last two equations in the preceding equation are the same as the last two equations in Equation (10).

Since the tangent and normal vectors are functions of the surface parameters, one may rewrite the preceding set of algebraic equations in a vector form as

$$\mathbf{E}(\mathbf{s}) = \mathbf{0} \tag{25}$$

where $\mathbf{E}$ is the vector of nonlinear algebraic equations. These nonlinear algebraic equations can be solved for the surface parameters that define potential non-conformal contact points. To this end, a Newton–Raphson algorithm is employed. This requires evaluating the Jacobian matrix of the algebraic equations and iteratively solving the following system for each contact in order to determine Newton differences associated with the surface parameters:

$$\begin{bmatrix} \mathbf{t}_1^r \cdot \mathbf{t}_1^w & \mathbf{t}_1^r \cdot \mathbf{t}_2^w & \frac{\partial \mathbf{t}_1^r}{\partial s_1^r} \cdot \mathbf{r}^{wr} - \mathbf{t}_1^r \cdot \mathbf{t}_1^r & \frac{\partial \mathbf{t}_1^r}{\partial s_2^r} \cdot \mathbf{r}^{wr} - \mathbf{t}_1^r \cdot \mathbf{t}_2^r \\ \mathbf{t}_2^r \cdot \mathbf{t}_1^w & \mathbf{t}_2^r \cdot \mathbf{t}_2^w & \frac{\partial \mathbf{t}_2^r}{\partial s_1^r} \cdot \mathbf{r}^{wr} - \mathbf{t}_2^r \cdot \mathbf{t}_1^r & \frac{\partial \mathbf{t}_2^r}{\partial s_2^r} \cdot \mathbf{r}^{wr} - \mathbf{t}_2^r \cdot \mathbf{t}_2^r \\ \frac{\partial \mathbf{t}_1^w}{\partial s_1^w} \cdot \mathbf{n}^r & \frac{\partial \mathbf{t}_1^w}{\partial s_2^w} \cdot \mathbf{n}^r & \frac{\partial \mathbf{n}^r}{\partial s_1^r} \cdot \mathbf{t}_1^w & \frac{\partial \mathbf{n}^r}{\partial s_2^r} \cdot \mathbf{t}_1^w \\ \frac{\partial \mathbf{t}_2^w}{\partial s_1^w} \cdot \mathbf{n}^r & \frac{\partial \mathbf{t}_2^w}{\partial s_2^w} \cdot \mathbf{n}^r & \frac{\partial \mathbf{n}^r}{\partial s_1^r} \cdot \mathbf{t}_2^w & \frac{\partial \mathbf{n}^r}{\partial s_2^r} \cdot \mathbf{t}_2^w \end{bmatrix} \begin{bmatrix} \Delta s_1^w \\ \Delta s_2^w \\ \Delta s_1^r \\ \Delta s_2^r \end{bmatrix} = - \begin{bmatrix} \mathbf{t}_1^r \cdot \mathbf{r}^{wr} \\ \mathbf{t}_2^r \cdot \mathbf{r}^{wr} \\ \mathbf{t}_1^w \cdot \mathbf{n}^r \\ \mathbf{t}_2^w \cdot \mathbf{n}^r \end{bmatrix} \tag{26}$$

Convergence is achieved when the norm of the violation of the algebraic equations or the norm of the Newton differences is less than a specified tolerance.

Having determined the vector of the surface parameters, the penetration can be calculated using the third equation of Equation (10) as

$$\delta = \mathbf{r}^{wr} \cdot \mathbf{n}^{r} \tag{27}$$

If the surfaces penetrate, normal contact forces can be calculated using Hertz's contact theory, while the creep forces can be calculated using Kalker's USETAB routine [12, 13]. The generalized normal and creep forces associated with the system generalized coordinates are determined and introduced to the multibody system dynamic equations of motion. In the evaluation of the normal contact force, as an alternate to the use of the Hertzian component that is a function of the indentation, a damping force proportional to the time derivative of indentation can be included. The expression of the normal force used in this investigation is given by [9]:

$$F = F_h + F_d = -K_h \delta^{3/2} - C\dot{\delta}|\delta| \tag{28}$$

where δ is the indentation, F_h is the Hertzian (elastic) contact force, F_d is the damping force, K_h is the Hertzian constant that depends on the surface curvatures and the elastic properties, and C is a damping constant. The velocity of indentation $\dot{\delta}$ is evaluated as the dot product of the relative velocity vector between the contact points on the wheel and rail and the normal vector to the surface at the contact point. The reason for including the factor $|\delta|$ in the damping force is to guarantee that the contact force is zero when the indentation is zero.

4.2. Use of Nodal Search (ECF-N)

An alternate for using the ECF-A method that employs algebraic equations is to define the profile of the wheel and rail using discrete nodal points [9, 14]. The distance between those nodes can be calculated to determine which nodes can come in contact. The use of this method has the advantage that it does not require a certain degree of smoothness of the surfaces. It has, however, the disadvantage that the change in the lateral surface parameters of wheel and rail is not smooth since the contact is assumed to occur at discrete nodal points. When the contact jumps from one node to the neighboring one, a small jump in the relative velocity between the wheel and the rail at the contact point is expected. This small jump leads, in some examples, to discontinuity of the creepages. Since the creepage coefficients that enter into the calculation of the creep forces are very high, the change in the contact locations resulting from the use of the nodal search leads to high impulsive forces. As discussed in [9], the nodal search for the contact points consists of the following three steps:

1. Calculation of the rail arc length s_1^r traveled by the wheel. The parameter s_1^r defines the rail cross section in which the points of contact are located.
2. Calculation of the wheel angular parameter s_2^w. The parameter s_2^w defines the wheel diametric section in which the points of contact are located.
3. Search for the contact points. In this phase the rail parameter s_2^r and the wheel parameter s_1^w of the points of contact are determined. This phase of the search starts once the sections of the wheel and rail in which the contact points are located are determined. The exact position of the contact points is determined in this phase of the search.

In order to determine the arc length traveled by the wheel, a selected point Q on the center of the wheel is used first to determine the rail space curve parameter s_1^r. It is assumed that the rate of change of the rail parameter s_1^r is equal to the projection of the velocity of this point on the tangent along the

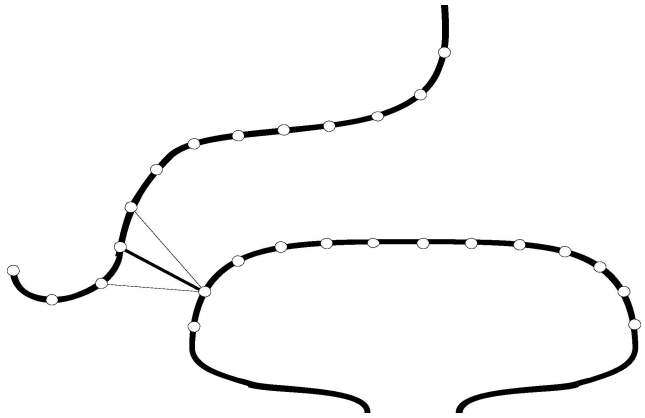

Figure 11. The surface nodal points.

longitudinal rail direction, that is

$$\dot{s}_1^r = \dot{\mathbf{r}}_Q^{wT} \cdot \mathbf{t}_1^r \tag{29}$$

where $\dot{\mathbf{r}}_Q^w$ is the global velocity vector of point Q, and $\mathbf{t}_1^r$ is the longitudinal tangent to the rail. The preceding differential equation is solved simultaneously with the differential and algebraic equations of the multibody system in order to determine s_1^r that is used for the search for the point of contact between the wheel and the rail. Clearly, one needs to introduce a number of arc length first order differential equations equal to the number of wheels in the dynamic model. Note that the ECF-A method does not require introducing these first order differential equations since the arc length traveled by the wheel is readily available from the solution of the algebraic equations.

In order to determine the points of contact between the wheel and the rail, the global position vectors of the nodal points that define the wheel and rail profiles are determined [9]. The distance between the points on the wheel and the points on the rail, as shown in Figure 11, are calculated and used with a user specified tolerance criterion to determine the points of contact. Since this search for the contact points can lead to a very large number of contact points, an optimized procedure that improves the computational efficiency is adopted. The contact points are grouped in batches. A batch is a collection of sequence of pairs of points on the wheel and rail that have non-zero penetration. While the algorithm developed allows for an arbitrary number of contact batches, a limit of two contact batches is assumed in the numerical investigation presented in this paper. The two points (one on the wheel and one on the rail) that lead to the maximum indentation are selected as the points of contact for any given batch. The number of points of contact between the wheel and the rail is equal to the number of the contact batches. That is, the algorithm used to search for the contact points allows for multiple contacts between the wheel and the rail. Once the contact points are determined, an elastic force model similar to the one presented for the ECF-A method can be used.

4.3. Comparison between the Two Elastic Contact Formulations

Once the normal and creep contact forces are determined, the augmented form of the equation of motion of the multibody system can be written as [12]:

$$\begin{bmatrix} \mathbf{M} & \mathbf{C}_\mathbf{q}^\mathbf{t} \\ \mathbf{C}_\mathbf{q} & \mathbf{0} \end{bmatrix} \begin{bmatrix} \ddot{\mathbf{q}} \\ \boldsymbol{\lambda} \end{bmatrix} = \begin{bmatrix} \mathbf{Q} \\ \mathbf{Q}_c \end{bmatrix} \tag{30}$$

where $\mathbf{M}$ is the system mass matrix, $\mathbf{C}_\mathbf{q}$ is the Jacobian matrix of the non-contact kinematic constraints, $\mathbf{q}$ is the vector of the system generalized coordinates, $\boldsymbol{\lambda}$ is the vector of Lagrange multipliers, $\mathbf{Q}$ is a vector that includes external, applied contact, creep, and centrifugal and Coriolis forces, and $\mathbf{Q}_c$ is the vector that results from the differentiation of the constraint equations twice with respect to time, that is

$$\mathbf{C}_\mathbf{q}\ddot{\mathbf{q}} = \mathbf{Q}_c \tag{31}$$

The vector of the kinematic constraint equations $\mathbf{C}(\mathbf{q}, t) = \mathbf{0}$ describes mechanical joints as well as specified motion trajectories that include driving constraints. Such driving constraints include the specified forward velocity of the wheel sets. In the elastic contact formulations, the vector $\mathbf{C}$ does not include any contact constraints.

Crucial to the success of any elastic force model used in the dynamic simulation of the interaction between the wheel and the rail is the accurate prediction of the rail arc length traveled by the wheel. As previously pointed out, in the ECF-A method this arc length is determined by solving algebraic equations, while the ECF-N method allows for such an accurate prediction by introducing an arc length first order differential equation that depends nonlinearly on the wheel generalized coordinates and the rail geometry. This first order differential equation, which is defined by Equation (29), is integrated simultaneously with the state equations obtained for the wheel/rail system using Equation (30). The numerical integration of this new combined system of equations defines the system generalized coordinates and velocities as well as the rail arc length s_1^r traveled by the wheel.

In order to compare between the results obtained in the two methods (ECF-A and ECF-N) discussed in this section, we consider the suspended wheel set example examined in the preceding section. This example is solved again using the two elastic contact formulations ECF-A and ECF-N. Figures 12 and 13 show the lateral and yaw displacements of the wheel set; while Figure 14 Shows the normal component of the normal force acting on the right wheel. The results presented in these figures show a good agreement between the solutions obtained using the two different elastic methods.

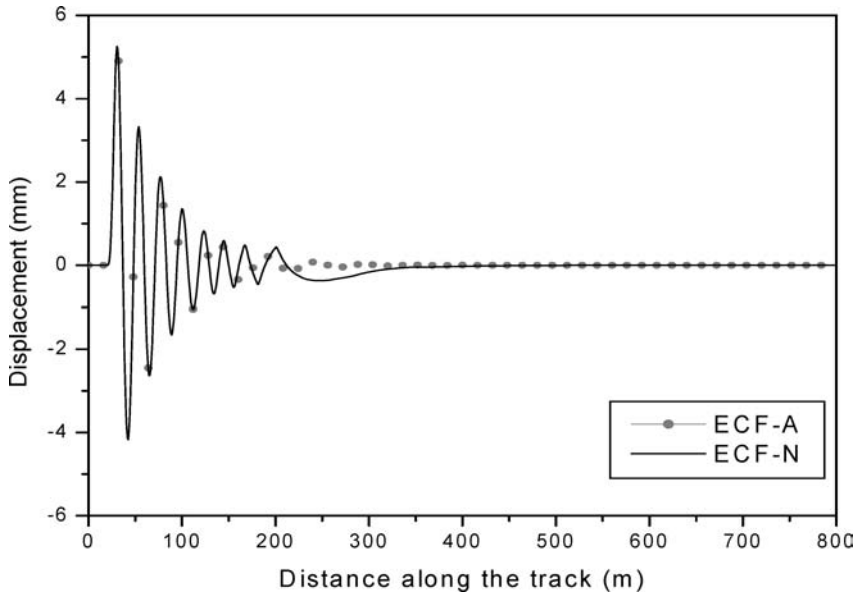

Figure 12. Lateral displacement of the wheel set.

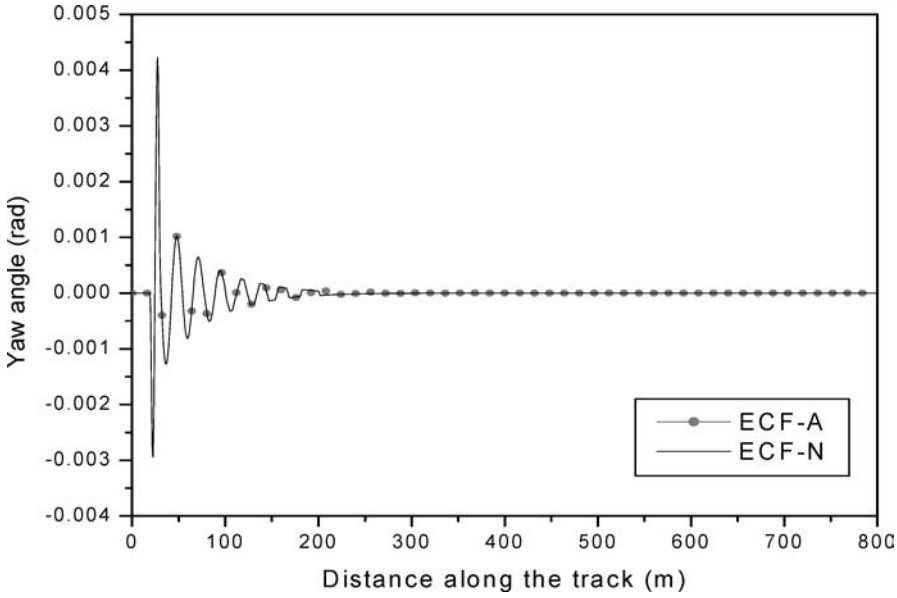

Figure 13. Yaw angle of the wheel set.

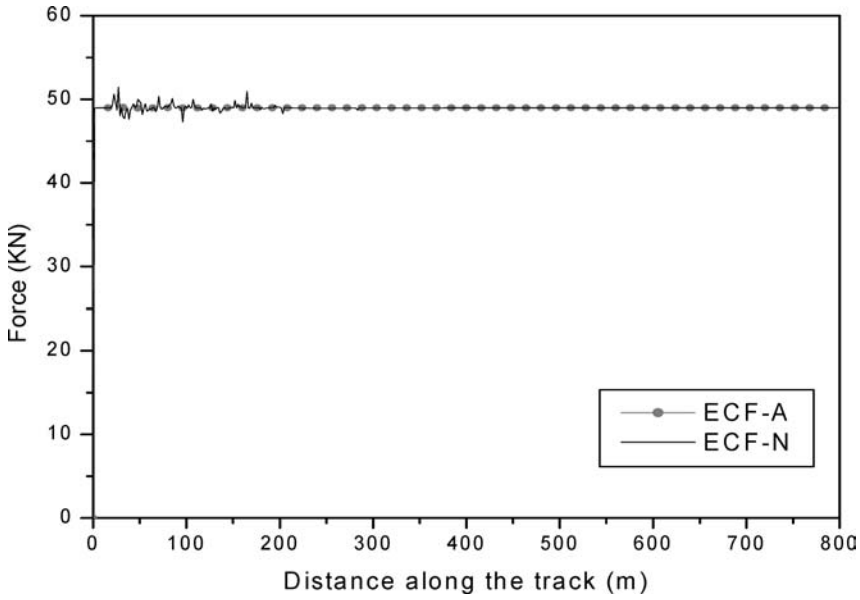

Figure 14. Normal contact forces of the wheel set.

5. Vehicle Model

In this section, we consider a complete vehicle model shown in Figure 15 in order to compare between the results obtained using the embedded contact constraint method (ECCF) and the elastic contact formulations (ECF-A) that employs algebraic equations to determine the location of the contact point.

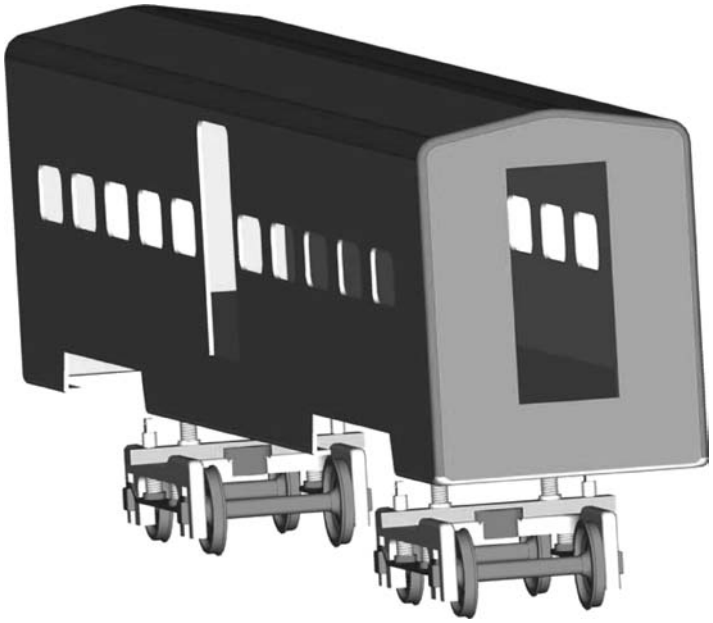

Figure 15. Vehicle model.

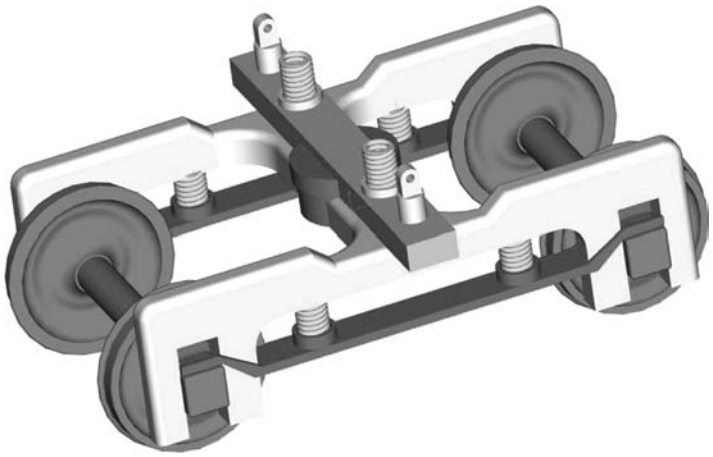

Figure 16. The components of the truck.

The vehicle that consists of two trucks and a car body is assumed to travel on a tangent track. Each truck consists of two wheel sets, two equalizer bars, a frame and a bolster as shown in Figure 16. The front wheel sets of the leading and trailing truck are assumed to have a constant forward velocity ($V = 20$ m/s). The track is assumed perfectly tangent with two vertical bumps as shown in Figure 17. The dimensions and inertia properties of this model are the same as presented in [15]. Figure 18 shows the lateral displacement of the rear trailing wheel set, while Figure 19 shows the vertical displacement. Figure 20 shows the normal forces acting on the right wheel of the leading wheel set of the leading truck. It can be seen that there is in general a good agreement between the constraint and the elastic formulations.

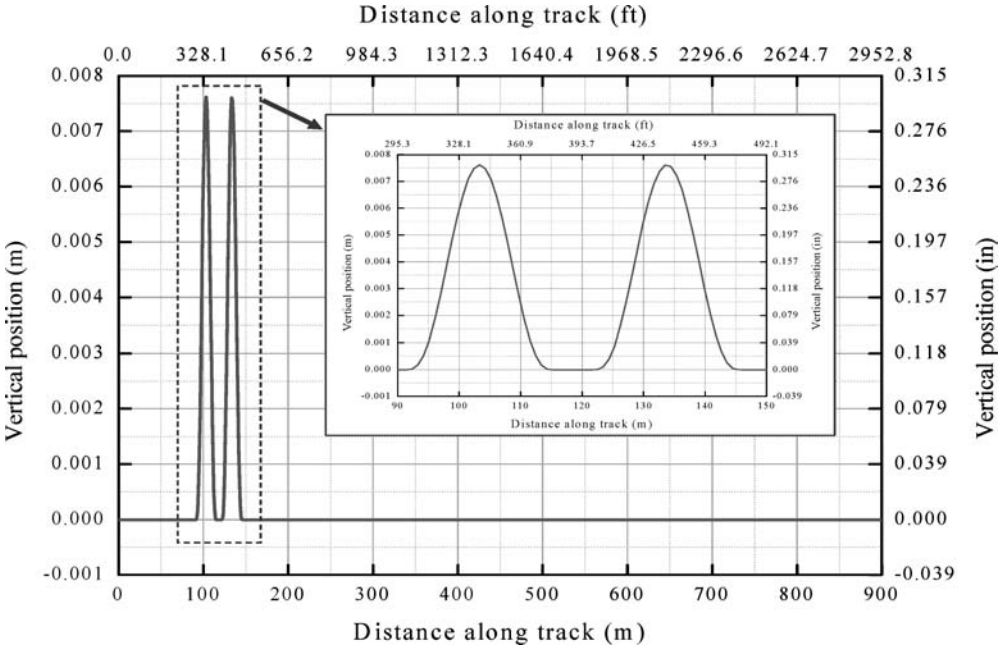

Figure 17. Track with vertical bump.

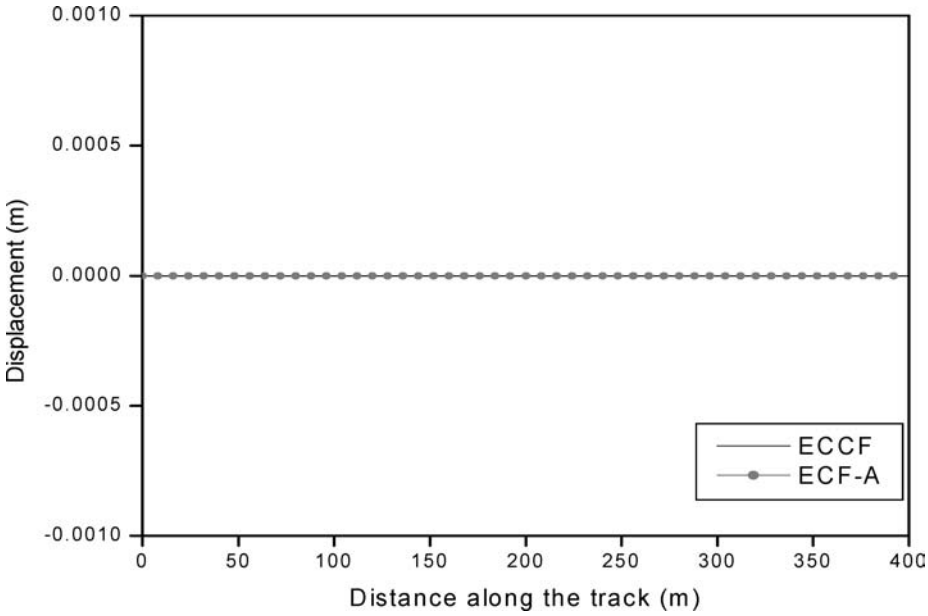

Figure 18. Lateral displacement of the rear wheel set of the trailing truck.

6. Curving Behavior and Two-Point Contact

The results presented in the preceding section were obtained using a tangent track. In this section, the results obtained using the constraint and elastic formulations (ECCF and ECF-A) are compared when the vehicle negotiates a curved track. In the analysis of the curving behavior, the effect of the

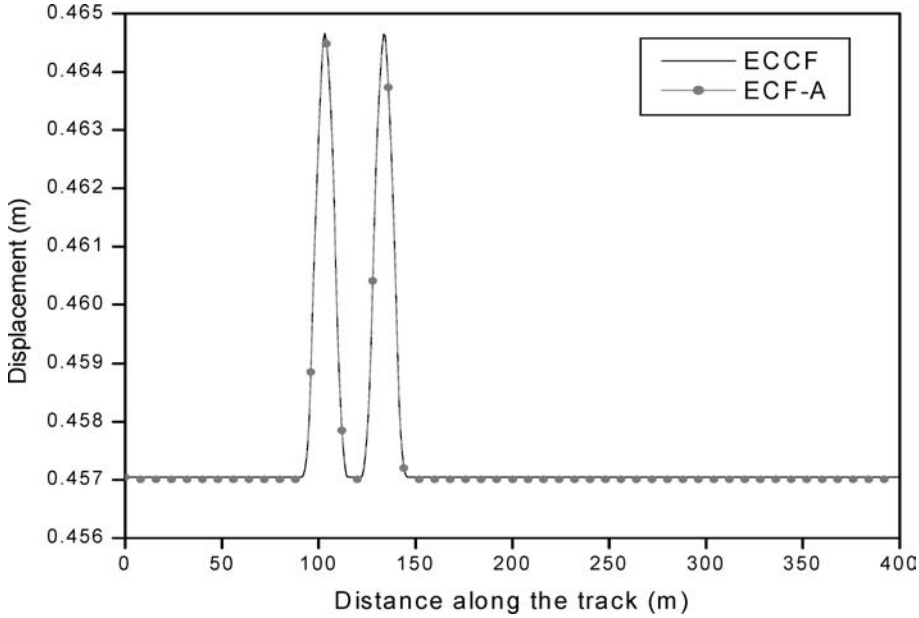

Figure 19. Vertical displacement of the rear wheel set of the trailing truck.

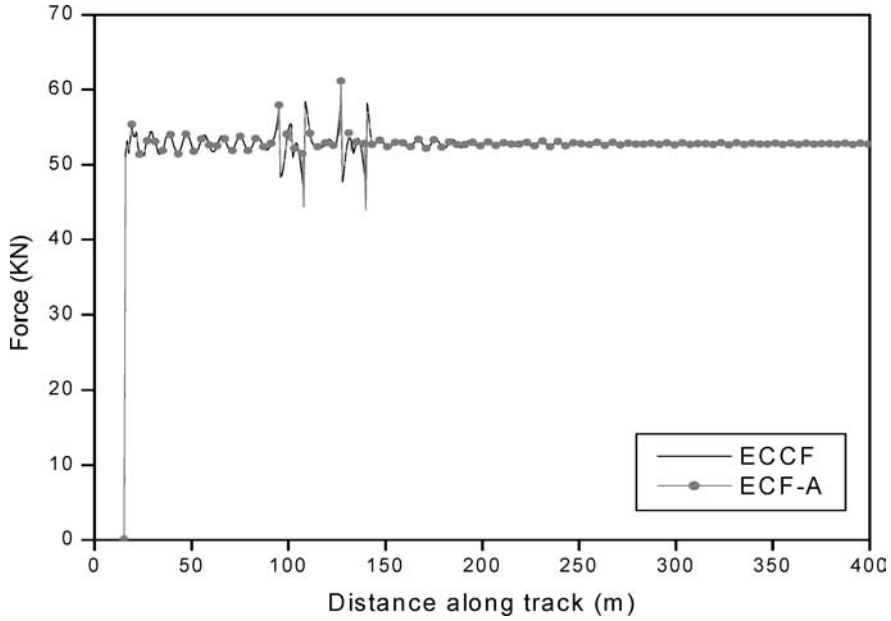

Figure 20. Normal contact force of the right wheel of the front wheel set of the leading truck.

forces due to flange contact is important and must be taken into consideration. The procedure used in this investigation to determine the second point of contact on the flange of the wheel is based on determining two points on the rail profile and the wheel flange that have the shortest distance. The distance between the two points along the normal at the point of contact on the rail is calculated to determine whether or not penetration occurs. The procedure also allows for checking the lead and lag

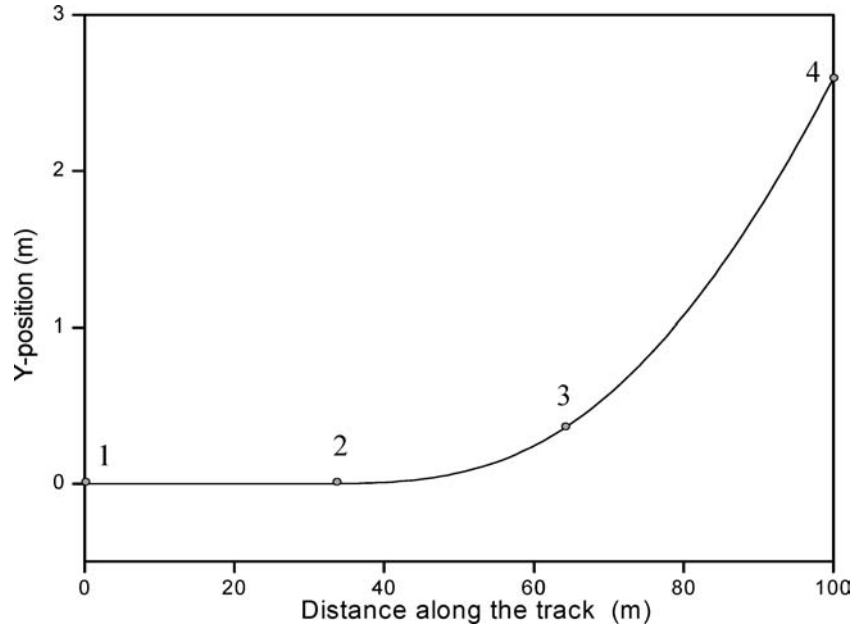

Figure 21. Curved track.

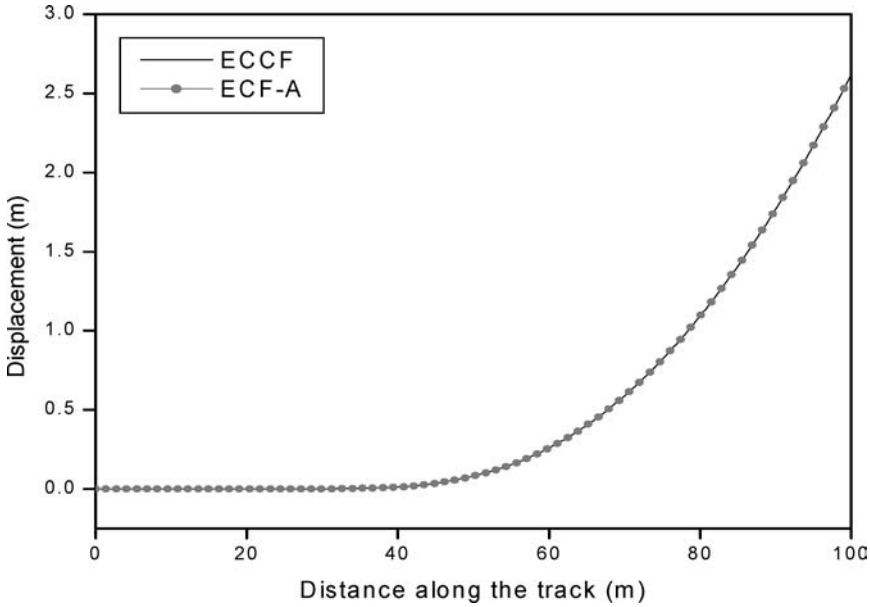

Figure 22. Car body lateral displacement.

contact using information on the wheel lateral displacement and orientation. If penetration occurs, a compliant force element similar to the one used for the elastic methods is used to define the normal contact force; that is, an elastic approach is always used to model the flange contact regardless of the method used to model the tread contact. In order to compare between the ECCF and the ECF-A methods when a vehicle negotiates a curved track, the track shown in Figure 21 is used. The data for this track are

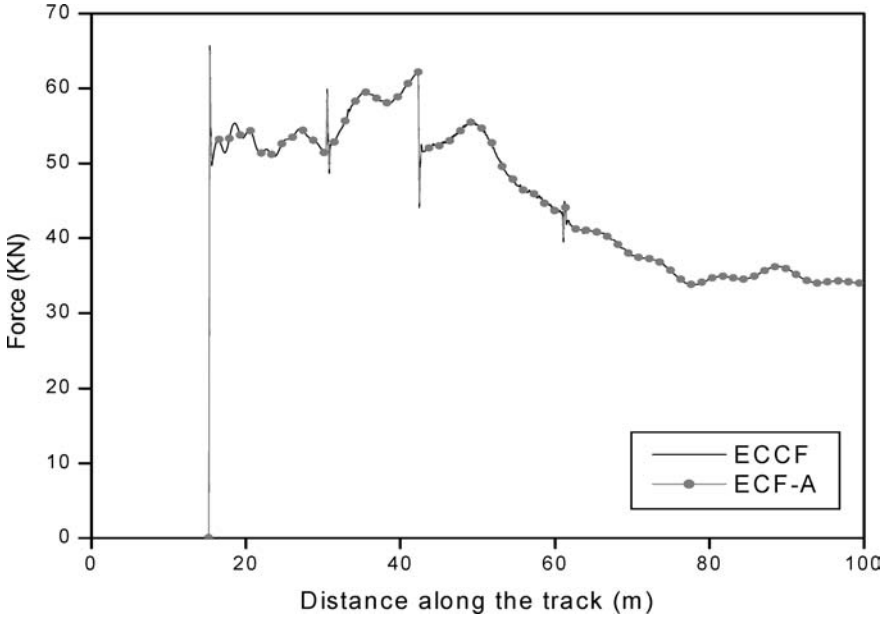

Figure 23. Normal contact force of the tread contact.

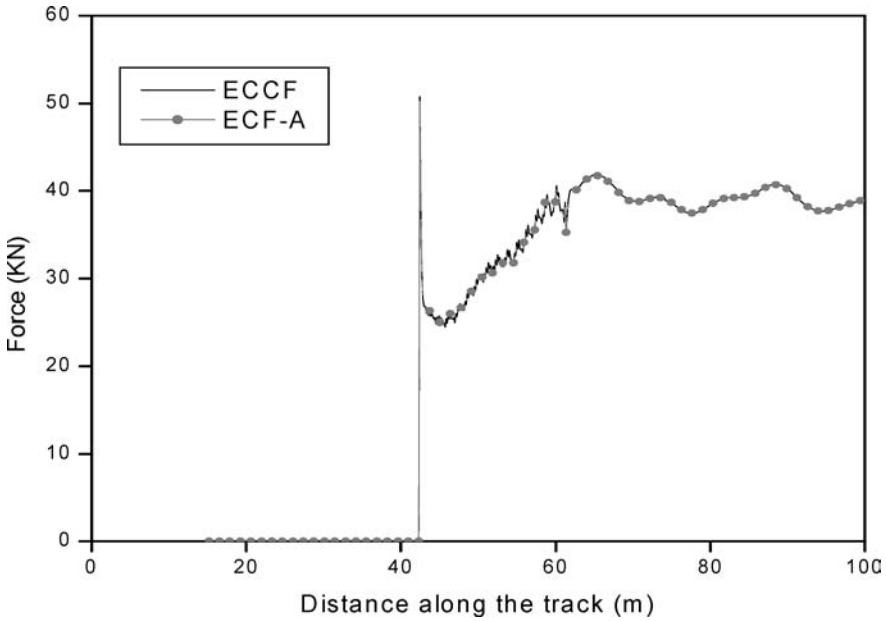

Figure 24. Normal contact force of the flange contact.

presented in Table 2. Figure 22 shows the lateral displacement of the vehicle described in the previous section when it travels on the curved track shown in Figure 21. Figures 23 and 24 show the components of the tread and flange normal contact force acting on the right wheel of the front axle of the leading truck.

Table 2. Track node data.

Node	Distance (ft.)	Curvature (deg.)	Superelevation (in)	Grade (%)
1	0	0	0	0
2	100	0	0	0
3	200	3	−3	0
4	350	3	−3	0

7. Summary and Conclusions

In this investigation, several nonlinear dynamic formulations for the analysis of the wheel/rail contact problems are discussed. Two contact constraint formulations (ACCF and ECCF) and two elastic contact formulations (ECF-A and ECF-N) are discussed. Each contact in the constraint formulations eliminates one relative degree of freedom between the wheel and the rail.

In the embedded contact constraint formulations (ECCF), the surface parameters are systematically eliminated leading to a reduced system of equations that do not explicitly include the contact constraint forces. Numerical results presented in this investigation show that there is a good agreement between the solution obtained using the embedded contact constraint method (ECCF) in which the surface parameters can not be used as degrees of freedom and the solution of the augmented contact constraint formulation (ACCF) that allows the selection of surface parameters as degrees of freedom. In the augmented contact constraint formulations (ACCF), the kinematic contact constraint equations are augmented to the system differential equations of motion. As demonstrated in this paper, the two contact constraint formulations, ECCF and ACCF, are equivalent, but require the use of different solution procedures.

The elastic formulations, on the other hand, do not impose any kinematic constraints on the motion of the wheel with respect to the rail, and therefore, the wheel is assumed to have six degrees of freedom with respect to the rail. The results obtained using the two elastic formulations (ECF-A and ECF-N) are also compared. Numerical experimentation showed that the ECF-A method that determines the location of the contact points by solving algebraic equations leads, in general, to smoother results as compared to the ECF-N method that uses nodal search to determine the contact points. As explained in the paper, the use of the nodal search in the ECF-N method can lead, in some examples, to non-smooth change in the lateral surface parameters, and as a consequence, the contact and creep forces can be impulsive as the results of very high creepage coefficients. It is important, however, to point out that the ECF-A method requires a certain degree of surface smoothness which is not required by the ECF-N method. The results of the constraint ECCF method and the elastic ECF-A method are compared using a full vehicle model traveling on tangent and curved tracks. In the case of the curved track, the effect of the forces of the second point of contact is taken into consideration. The results obtained show a good agreement between the solutions obtained using the constraint and the elastic methods.

Acknowledgement

The research presented in this investigation was supported by the Federal Railroad Administration.

References

1. De Pater, A. D., 'The geometrical contact between track and wheel set' , *Vehicle System Dynamics* **17**, 1988, 127–140.
2. Simeon, B., Fuhrer, C., and Rentrop, P., 'Differential algebraic equations in vehicle system dynamics ', *Survey on Mathematics in Industry* **1**, 1991, 1–37.
3. Kalker, J. J., 'Survey of wheel-rail rolling contact theory', *Vehicle System Dynamics* **8**(4), 1979, 317–358.
4. Knothe, K. and Bohm, F., 'History of stability of railway and road vehicle', *Vehicle System Dynamics* **31**, 1999, 283–323.
5. Iwnicki, S., *The Manchester Benchmarks for Rail Vehicle Simulation,* Swets & Zeitlinger, Lisse, The Netherlands, 1999.
6. Garg, V. K. and Dukkipati, R. V., *Dynamics of Railway Vehicle Systems,* Academic Press, Orlando, FL, 1984.
7. Shabana, A. A. and Sany, J. R., 'A survey of rail vehicle track simulations and flexible multibody dynamics', *Nonlinear Dynamics* **26**, 2001, 179–210.
8. Shabana, A. A. and Sany, J. R., 'An augmented formulation for mechanical systems with non-generalized coordinates: Application to rigid body contact problems', *Nonlinear Dynamics* **24**, 2001, 183–204.
9. Shabana, A. A., Zaazaa, E. K., Escalona, L. J., and Sany, J. R., 'Development of elastic force model for wheel/rail contact problems', *Journal of Sound and Vibration* **269**, 2004, 295–325.
10. Shabana, A. A., Berzeri, M., and Sany, J. R., 'Curved track modeling using the absolute nodal coordinate formulation', Technical Report No. MBS00-4-UIC, 2000, University of Illinois at Chicago, IL.
11. Pombo, J. and Ambrosio, J., 'A wheel/rail contact model for rail guided vehicles dynamics', in *Proceedings of ECCOMAS Thematic Conference on Advances in Computational Multibody Dynamics*, Lisboa, Portugal, 1–4 July 2003.
12. Kalker, J. J., 'Three-dimensional elastic bodies in rolling contact', Kluwer Academic Publishers, Boston, MA, 1990.
13. Kalker, J. J., 'Wheel-rail rolling contact theory', *Wear* **144**, 1991, 243–261.
14. Kik, W. and Piotrowski, J., 'A fast approximation method to calculate normal load at contact between wheel and rail and creep forces during rolling', in *Proceedings of 2nd Mini Conference on Contact Mechanics and Wear of Rail/Wheel System*, I. Zabory (ed.), TU Budapest, 1996.
15. Zaazaa, K., 'Elastic force model for wheel/rail contact in multibody railroad vehicle systems', Ph.D. Thesis, Department of Mechanical Engineering, University of Illinois at Chicago, Chicago, IL, 2003.